Nanoscale Upconversion for Oxygen Sensing

Kayla Presley,[a] Jinwoo Hwang,[a] Soshan Chang,[b] Richard Tilley,[b] Josh Collins,[c] Mariano Viapiano,[d] John Lannutti[a]
[a]Materials Science and Engineering, The Ohio State University, Columbus, OH 43210, USA
[b]School of Chemistry, UNSW Australia, Sydney NSW 2052, Australia
[c]Intelligent Materials Solutions, Inc., Princeton, NJ 08540
[d]Neuroscience and Physiology, State University of New York Upstate Medical University, Syracuse, NY 13210, USA

ABSTRACT: Optical oxygen sensors have many promising qualities but rely on excitation by violet or blue wavelengths that suffer from high levels of scattering and absorption in biological tissues. Here we demonstrate an alternative method using 980 nm near-infrared light to initially stimulate ceramic upconverting nanoparticles (UCNPs) contained within a novel form, electrospun core-shell fibers. The emission of the UCNPs excites a molecular optical oxygen sensor, the subsequent phosphorescent emission being dynamically quenched by the presence of molecular oxygen. The potential for use of such an energy transfer within electrospun fibers widely used in biological applications is promising. However, current knowledge of such 'handshake' interactions is limited. Fiber-based carriers enabling such optical conversions provide unique opportunities for biosensing as they recapitulate the topography of the extracellular matrix. This creates a wide array of potential theranostic, fiber-based applications in disease diagnosis/imaging, drug delivery and monitoring of therapeutic response. Using a fiber-based vehicle, we observed gaseous oxygen sensing capabilities and a linear Stern-Volmer response allowing highly accurate calibration. Configurational aspects were also studied to determine how to maximize the efficiency of this 'handshake' interaction.

Keywords: upconversion; in vivo oxygen sensing; electrospinning; upconverting nanoparticles; polysulfone; polycaprolactone

Graphical abstract:

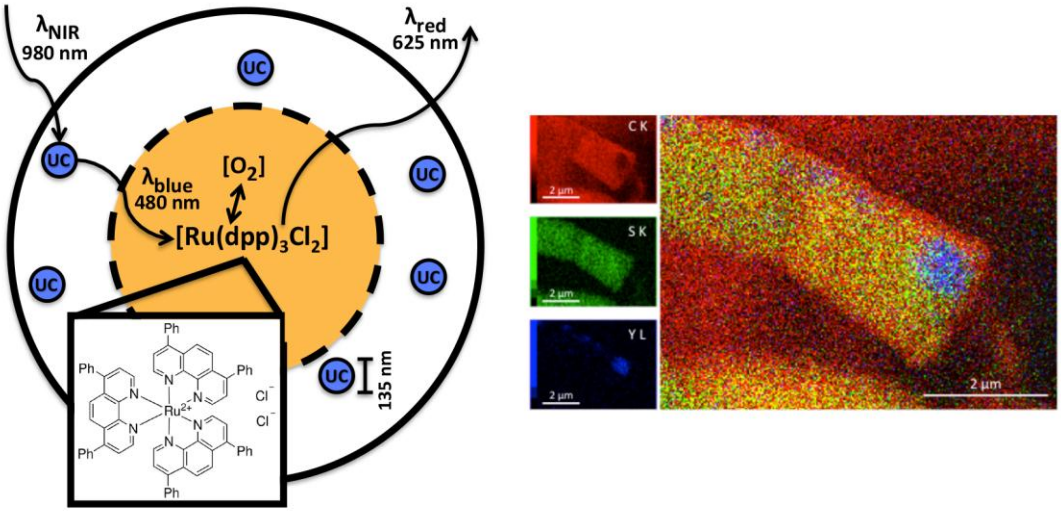

1. Introduction

In this paper we demonstrate that NIR stimulation of UCNPs contained within the shell of electrospun core-shell fibers can be used to produce blue (480 nm) light which in turn excites core-bound $Ru(dpp)_3Cl_2$ to produce a red (~625 nm) phosphorescence dynamically regulated by the amount of molecular oxygen present.[1,2] We refer to this overall process as a 'handshake' interaction between the UCNPs and the Ru complex to distinguish it from radiationless luminescence resonance energy transfer (LRET).[3]

Monitoring of local deep tissue oxygen concentrations in real-time could be achieved via this configuration, and such abilities are sought after in many biomedical applications. A potential specific application is the identification of hypoxic regions

generated by cancerous tumors either *in vivo* or *in vitro*.[4] This ability would be especially relevant in detecting recurrence of glioma brain tumors. Gliomas often recur either at the original tumor site or within 2-3 cm.[5–7] However, gliomas must be at least 2.8 mm in diameter to be detectable by magnetic resonance imaging (MRI).[8] Optical techniques of sensing local oxygen concentration could potentially be used to detect much smaller recurrences of gliomas because these tumors contain highly hypoxic regions.[9] Tumor oxygenation is a known indicator of metastatic potential,[10] because hypoxia triggers mechanisms of tumor cell dispersion and apoptotic resistance.[11–13] As a result, traditional radiation and chemotherapy treatments are often ineffective in attacking cells found in such regions of low oxygen content.[14,15] In fact, both hyperbaric oxygen therapy and oxygen diffusion-enhancing compounds, such as trans sodium crocetinate (TSC), have been used to re-oxygenate hypoxic tumor tissue to render it more sensitive to radiation.[16]

Due to their unique optical properties, upconverting nanoparticles (UCNPs) have enjoyed growing interest in such novel applications.[17,18] Via a multi-photon process, UCNPs can absorb near-infrared (NIR) light and emit visible light.[19,20] This anti-Stokes process makes them especially attractive for bioimaging applications due to the absence of 'blinking,' the lack of background auto-fluorescence, and the increased penetration depth characteristic of NIR light.[17,21,22] NIR can penetrate tissue more easily than visible light due to decreased levels of absorption and scattering. Rayleigh scattering decreases with increased wavelengths, while absorption is also low in the NIR region.[23] UCNPs are excited by 980 nm NIR light which falls within the 600-1300 nm "optical window" for enhanced light transmission through biological tissue.[22] This window is bound by high pigment (i.e., hemoglobin) absorption at lower visible wavelengths and strong water absorption at higher wavelengths.[22,24]

The optical properties of UCNPs may also make them useful for sensing applications. While a variety of luminescent probes can be used in sensors (i.e., for measuring local chemical concentrations), their reliance on visible wavelengths limits their applications in visually opaque biological environments or in tissues that are anatomically isolated and difficult to interrogate by non-invasive methodologies, such as the central nervous system. By using UCNPs in conjunction with luminescent probe molecules, the sensing of local chemical conditions can be extended to biological applications in which light energy must travel through a thick layer of tissue (including high-scattering tissue such as bone) to excite a chemical sensor.

One particularly useful application of UCNPs is the local excitation of co-localized oxygen-sensitive probes (i.e. organometallic complexes and metalloporphyrins), which exhibit a luminescence quenched in proportion to the amount of oxygen present. We have incorporated UCNPs ($LiYF_4$:Yb,Tm) with the oxygen-sensitive molecule tris (4,7-diphenyl-1,10-phenanthroline) ruthenium (II) dichloride ($Ru(dpp)_3Cl_2$) into electrospun core-shell fibers. Despite the longer lifetimes and, therefore, increased oxygen-sensitivity of such porphyrins as palladium (II) and platinum (II) tetrakis(pentafluorophenyl)porphyrin (PdTFPP and PtTFPP),[4,25] $Ru(dpp)_3Cl_2$ was chosen due to its broad absorption peak that overlaps efficiently with the upconverter emission at 480 nm.[26–28] The detailed electronic interactions between the UCNPs and the ruthenium complex are shown in Figure 1. The $LiYF_4$:Yb,Tm contains sensitizer and activator ions, Yb^{3+} and Tm^{3+}, respectively. Yb^{3+} allows for 980 nm light to be absorbed

(by its $^2F_{5/2} \leftarrow {}^2F_{7/2}$ transition), while Tm^{3+} allows for the emission of blue light (by its $^1G_4 \rightarrow {}^3H_6$ and $^1D_2 \rightarrow {}^3F_4$ transitions).[1] The oxygen-sensitive $Ru(dpp)_3Cl_2$ then absorbs blue light radiatively emitted by the UCNPs to undergo a metal-to-ligand charge transfer in which a *d* orbital Ru electron is raised into a π^* ligand orbital. The subsequent decay results in a red (~625 nm) emission quenched by the presence of oxygen to dynamically regulate the ruthenium complex's phosphorescence.[2]

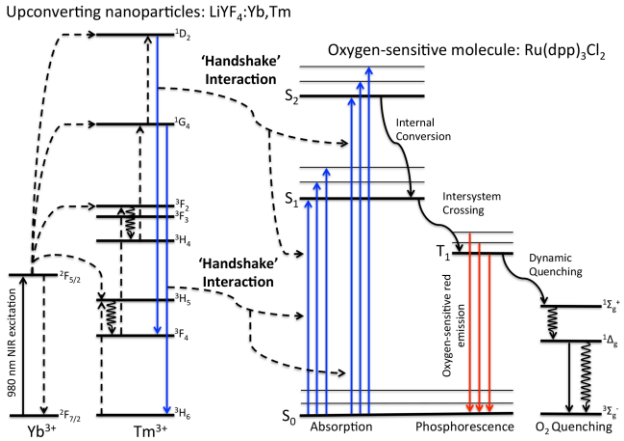

Figure 1: Energy levels depicting the electronic 'handshake' between $LiYF_4$:Yb,Tm upconverting nanoparticles and $Ru(dpp)_3Cl_2$.

To demonstrate this concept using a widely utilized biomaterial form, we incorporated UCNPs and an oxygen-sensitive complex into core-shell electrospun fibers with the goal of fabricating a nanoscaled carrier that could potentially be introduced in biological systems for long-term, minimally invasive, optical interrogation. In this method, multiple feed systems are utilized in the electrospinning process to create two separate flows each containing different polymer-based solutions. One solution becomes the core, the other the shell. A representative cross-section of a coaxial fiber is shown in Figure 2. These core-shell electrospun polymeric fibers are an ideal matrix for several reasons. In general, electrospun fibers are useful for biological applications due to their biomimetic topography and their greatly enhanced surface-to-volume ratio.[29] We have shown that the small scale and increased surface area imparted by the fiber morphology greatly decreases the response time relative to these film counterparts in oxygen sensing applications.[30] Additionally, core-shell electrospinning allows polymers that could not normally be easily electrospun to be incorporated as a 'core.'[31] Core-shell polymers have also been used in drug release applications and are of growing interest in biological applications due to the ability to easily design and select a biocompatible 'shell' that shields cells from both the chemistry and the contents of the core.[29] The core-shell structure offers flexibility in the placement of the UCNPs and the oxygen-sensitive complex, and a choice must be made as to whether to collocate or separate these individual components based on their effects on sensor performance. Since the dimensionality of the system components are nanoscaled, diffusional equilibrium is obtained within microseconds whether the components are either collocated or separated into the core and shell.

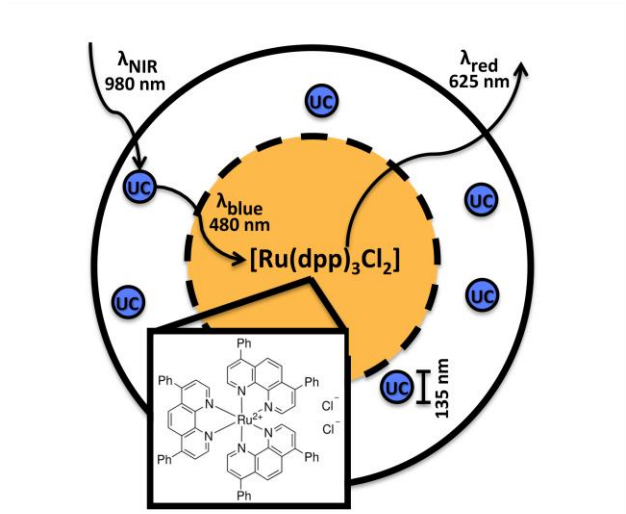

Figure 2: Cross-section depicting the targeted core-shell fibers. Note that 'UC' denotes upconverting nanoparticles in this schematic.

Current combinations of UCNPs and optical sensing molecules are limited but some efforts have been carried out.[32–37] Achatz at al. studied the upconversion of NIR light by $NaYF_4$:Yb,Tm into wavelengths suitable for the excitation of an oxygen-sensitive iridium complex in an ethyl cellulose film.[34] Lv et al. and Liu et al. recently demonstrated this idea in a nanoparticle form, where luminescence resonance energy transfer occurs between an upconverting nanoparticle and oxygen-sensitive molecules contained within its shell.[32,37] However, many configurational aspects of the 'handshake' interaction have not been studied, and the focus has exclusively been on polymer films or nanoparticles as carriers. In this work, we utilized a combination of experimental and analytical methods to study the 'handshake' interaction and analyze how it can be used effectively to create electrospun oxygen sensors for biological applications.

Spectroscopic techniques were used to evaluate the performance of core-shell configurations. Their performance was assessed in terms of intensity of output, gaseous oxygen sensing abilities, response time and resistance to photobleaching. The sensor morphology and the origins of this 'handshake' interaction were also assessed via other methods. Scanning electron microscopy (SEM) was used to study the fiber morphology and confirm the presence of UCNPs within the core-shell fibers. Confocal luminescence was used to study the visual output of the UCNPs contained within the fibrous morphology. Cathodoluminescence transmission electron microscopy (TEM-CL) provided a high spatial resolution enabling us to directly compare CL images and TEM images in assigning the structural origin of the observed luminescence.

2. Materials and Methods

2.1 Materials

PSU (M_n ~16,000) and PCL (M_n ~ 70,000–90,000) were purchased from Sigma-Aldrich (St. Louis, MO, USA). 1,1,1,3,3,3-hexafluoro-2-propanol (HFP) was acquired

from Oakwood Products (West Columbia, SC, USA), while dichloromethane (DCM) was obtained from Fisher Scientific (Pittsburgh, PA, USA). $LiYF_4$:Yb,Tm (~135 nm) nanoparticles were acquired from Intelligent Material Solutions (Princeton, NJ, USA), and tris (4,7-diphenyl-1,10-phenanthroline) ruthenium (II) dichloride ($Ru(dpp)_3Cl_2$) was purchased from Frontier Scientific (Logan, UT, USA).

2.2 Fabrication of electrospun core-shell fibers

The 'core' solutions were made by adding 12 wt% PSU pellets to a 50:50 (by weight) mixture of DCM and HFP. The 'shell' solutions were made by adding 5 wt% PCL to HFP. For the first sample (S1), $LiYF_4$:Yb,Tm and $Ru(dpp)_3Cl_2$ were added to the core solution with weight ratios of 8:100 and 5:1000 (versus the weight of PSU), respectively. For the second sample (S2), $Ru(dpp)_3Cl_2$ was added to the core solution, while $LiYF_4$:Yb,Tm was added to the shell. The third sample (S3) contained $LiYF_4$:Yb,Tm in the core and $Ru(dpp)_3Cl_2$ in the shell. The weight of each component in the final product was kept constant. All of these solutions were continuously mixed until dissolved.

These solutions were electrospun using a coaxial needle (inner needle: 22 gauge, outer needle: 14 gauge). The flow rates for the 'core and 'shell' solutions were set at 2 and 4 mL/hr, respectively. The distance between the needle tip and collecting plate was kept constant at 20 cm,[38] and 25 kV was used as the applied voltage. Each scaffold was electrospun for 20 minutes and then placed in a vacuum afterwards to remove any remaining HFP and DCM.[39] The samples were stored in a desiccator under darkness.

2.3 Characterization

A JEOL (Tokyo, Japan) 6500F field emission scanning electron microscope (SEM) operated at 15 kV with energy dispersive x-ray spectroscopy (EDS) capabilities was used to characterize fiber morphology and nanoparticle dispersion. TEM-CL experiments were performed on the sample using a FEI Titan Scanning TEM (STEM) operated at 80 kV and equipped with a Gatan Vulcan CL detector. TEM-CL uses an angstrom-size electron probe and provides CL spectra with both high energy and spatial resolution beyond the limits of conventional photoluminescence.[40] We used this capability to acquire CL data from individual, isolated core-shell fibers. STEM high-angle annular dark field (HAADF) images were simultaneously acquired with CL data for reference. The fibers were spun directly onto standard Cu mesh grids for TEM observation. Electron beam exposure can lead to carbon contamination of the fiber surface; we adjusted the CL acquisition time to avoid significant contamination build-up during the experiment.

Confocal photoluminescence images were taken using a Leica (Buffalo Grove, IL, USA) TCS SP5 inverted Confocal and Multiphoton Microscope (Mannheim, Germany) equipped with a Spectra-Physics Mai Tai HP 2-photon excitation laser (Mountain View, CA, USA) tunable from 720 –1040 nm. The photomultiplier tube detectors were tuned to detect +/- 20nm wavelengths around the desired peak emissions of 480 nm and 630 nm, respectively.

2.4 Oxygen sensing performance

A JAZ Ocean Optics spectrometer (Dunedin, FL, USA) was used to test the optical properties of the scaffolds. The scaffolds were cut into small squares and placed into a cuvette before they were tested in transmission. An adjustable power 980 nm continuous diode laser from Dragon Lasers (Changchun, China) was used at 1.25 W (a net irradiance of 2.6 W/cm^2) for excitation.

Various ratios of oxygen/nitrogen gas were obtained using a proportioning multiple-gas flow meter from Aalborg (Orangeburg, NY, USA). For gaseous oxygen sensing, these mixtures were flowed into the cuvette, and the response was monitored using the spectrometer. The spectral response was measured at various oxygen concentrations in which 30 measurements were averaged to provide the net result.

The oxygen quenching of transition metal complexes, such as $Ru(dpp)_3Cl_2$, is governed by the Stern-Volmer equation. In this equation, the intensity of phosphorescent emission is designed by I, I_0 indicates the intensity in the absence of oxygen, K_{SV} is the Stern-Volmer quenching constant, and $[O_2]$ is the concentration of oxygen.

$$I_0/I = 1 + K_{SV}[O_2] \quad (1)$$

To measure response time, the gas flow was rapidly switched between nitrogen and oxygen every 20 seconds. The intensity of the $Ru(dpp)_3Cl_2$ emission peak as a function of time was analyzed to acquire the response and recovery times. To assess photostability, the emission was monitored for an hour under blue light excitation. This test was performed with the sample inside of a cuvette filled with phosphate buffered saline (PBS).

3. Results

3.1 Morphology and particle dispersion

Figure 3 shows the morphology of representative electrospun core-shell samples. Fig. 3A demonstrates the typical core-shell electrospun fiber morphology. The small dimensions of the fibers in conjunction with the high porosity impart the scaffold with a high surface area. The backscattered compositional contrast between the ceramic UCNPs and the polymer matrix in Fig. 3B clearly demonstrates the presence of UCNPs within these fibers. If we consider that the average UCNP diameter is ~135 nm, some areas clearly appear to contain aggregates of multiple UCNPs. Figs. 3C and 3D show a single fiber. The UCNPs within this fiber are demonstrated by a backscattered electron image (Fig. 3C) and EDS maps (Fig. 3D). EDS maps were constructed for carbon, sulfur and yttrium. Carbon is present throughout the entire fiber from both the PSU and the PCL. However, sulfur is a component of only the PSU core; therefore, the PCL shell can be distinguished by the relative absence of sulfur. The yttrium EDS map indicates the presence of the $LiYF_4$:Yb,Tm UCNPs. Note that these areas correspond strongly to the location of these UCNPs as demonstrated by the backscattered electron image of this area (Fig. 3C).

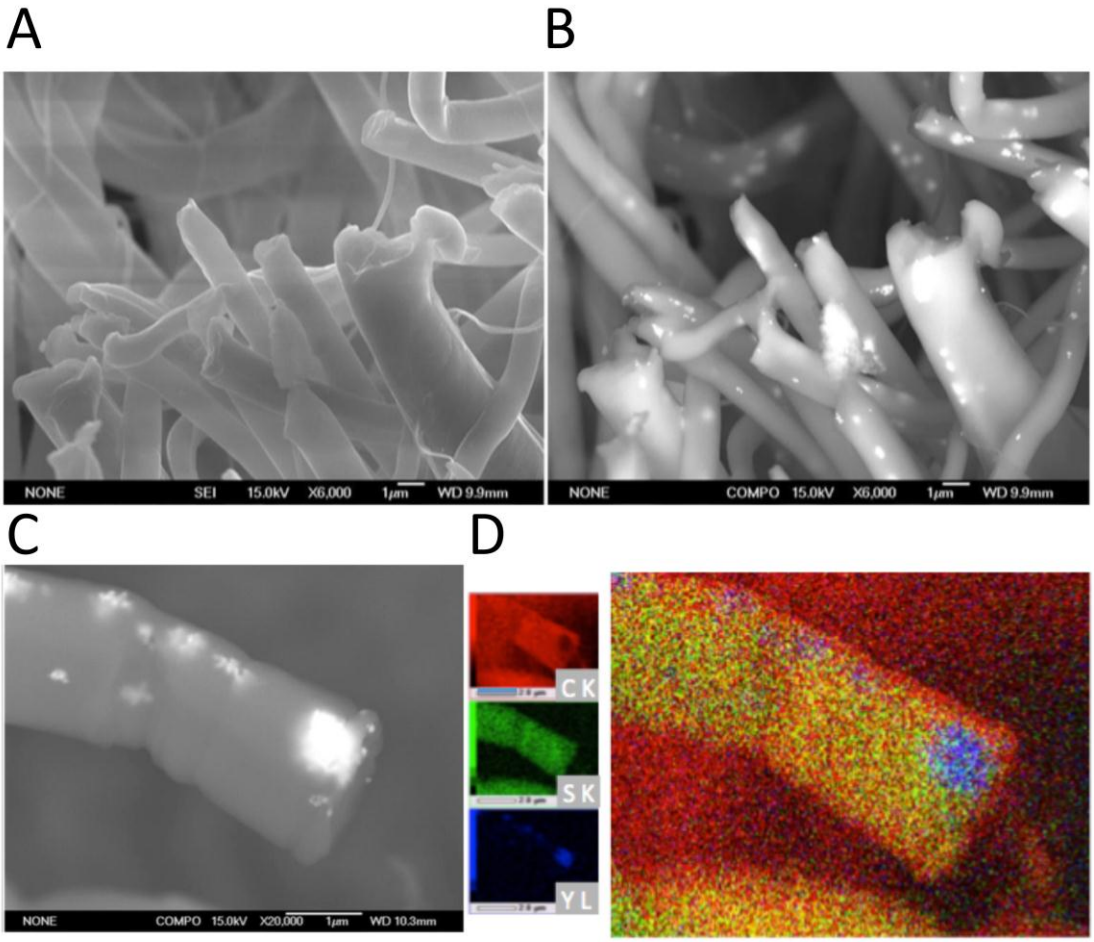

Figure 3: Representative core-shell sample with UCNPS in core (A) secondary electron SEM image (B)-(C) backscattered electron images and (D) EDS map.

3.2 TEM imaging and cathodoluminescent activity

High-resolution images and CL spectra from isolated fibers were acquired using STEM, and the results are displayed in Figure 4. Fig. 4A shows the HAADF image of a fiber containing $Ru(dpp)_3Cl_2$ in the core and individual UCNPs in the shell. The parallel lines observed within the fiber exterior are likely caused by aligned crystalline domains resulting from the rapid electrostatically driven extrusion and shrinkage characteristic of electrospinning.[41] Fig. 4B shows the CL spectrum obtained from the square area outlined in Fig. 4A. Two peaks, one at 625 nm and the other at 480 nm, are clearly identified indicating that the data captures the CL emitted by both the $Ru(dpp)_3Cl_2$ and the UCNPs. The peaks shown here likely result from direct electron excitation by the TEM beam, and therefore do not provide clear evidence of a 'handshake.' However, the CL result indicates that the blue emission from UCNPs is present and could likely induce red emission from the core by the proposed 'handshake' process. Since the penetration depth of TEM-CL is greater than 20 μm[40], it is safe to assume that the CL is from the

entire illuminated volume of the fiber (i.e. the volume inside the green box in Fig. 4A). This may explain why the peak at 480 nm is much smaller than the one at ~625 nm, because the $Ru(dpp)_3Cl_2$ molecules uniformly dispersed within the fiber core are being directly excited. The high-resolution STEM HAADF image in Fig. 4C confirms that the UCNPs retain good crystallinity within the fiber.

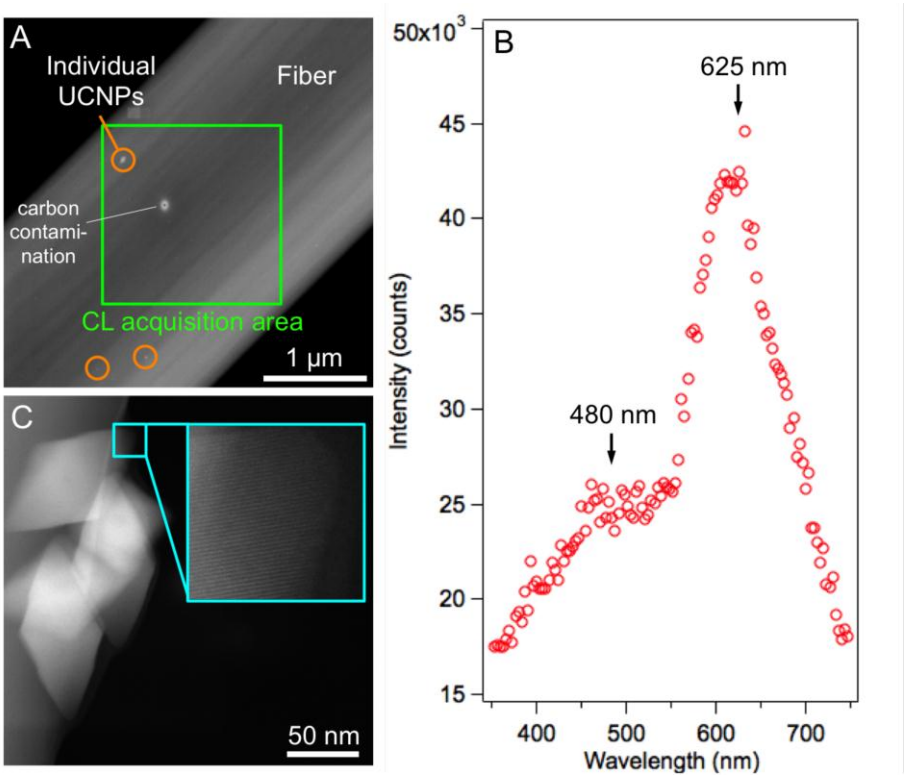

Figure 4: Representative core-shell sample (A) STEM HAADF image of an isolated fiber containing UCNPs. Individual UCNPs can be identified in the image (orange circles). (B) CL spectrum acquired from the green squared area in (A), showing peaks at 480 nm (blue) and 625 nm (red). (C) High resolution STEM image of a cluster of UCNPs. The inset shows the lattice fringes inside the particle, indicating good crystallinity.

3.3 Confocal luminescence

Figure 5 shows the confocal luminescence results from the PMT following pulsed wave 980 nm excitation of the $LiYF_4$:Yb,Tm UCNPs core-shell sample. The output of the dispersed $LiYF_4$:Yb,Tm nanoparticles contained within the ‘core’ of the fiber produces generalized areas of 480 nm emission visible in this image.

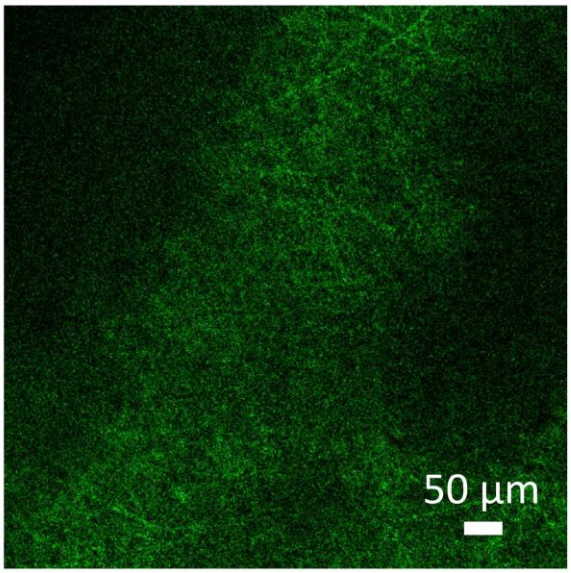

Figure 5: False-colored (in green) 480 nm output of $LiYF_4$:Yb,Tm UCNPs-containing core-shell fibers under vacuum following pulsed wave 980 nm excitation. The 480 nm output indicates a fibrous morphology. This widespread pattern of 480 nm emission shows that the $LiYF_4$:Yb,Tm UCNPs are generalized enough to provide continuous excitation of the $Ru(dpp)_3Cl_2$.

3.4 'Handshake' efficiency for different core-shell configurations

The placement of the UCNPs and Ru complex were varied to produce the three different core-shell configurations, S1, S2 and S3. S1 contains both $LiYF_4$:Yb,Tm and $Ru(dpp)_3Cl_2$ in the core. S2 contains $Ru(dpp)_3Cl_2$ in the core and $LiYF_4$:Yb,Tm in the shell, while S3 contains $LiYF_4$:Yb,Tm in the core and $Ru(dpp)_3Cl_2$ in the shell. The relative 'handshake' efficiency of these different configurations was analyzed by taking spectra in nitrogen and oxygen for each. By subtracting the nitrogen and oxygen spectra, the oxygen-sensitive emission alone could be characterized. Figure 6 shows the difference in oxygen-sensitive emission intensity for the various configurations. The least efficient configuration apparently occurred when both components were collocated in the core (S1). Location of the UCNPs in the core and $Ru(dpp)_3Cl_2$ in the shell (S3) provided the greatest efficiency.

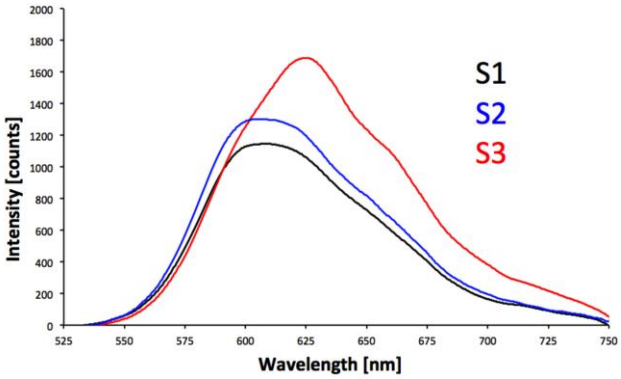

Figure 6: Subtracted N_2 and O_2 spectra for various core-shell configurations providing direct evidence for the 'handshake' process.

3.5 Gaseous oxygen sensing

Figure 7 displays the gaseous oxygen performance of the most efficient core-shell configuration (S3) plotted according to the Stern-Volmer equation (Equation 1). For gaseous oxygen sensing, a linear Stern-Volmer plot is observed with an R^2 value of 0.97356.

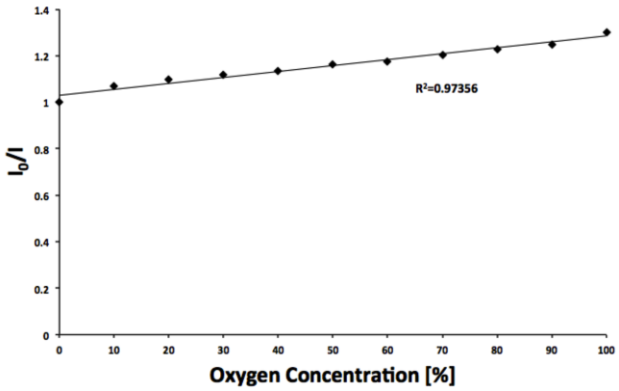

Figure 7: Gaseous oxygen sensing for PSU-PCL core-shell fibers with UCNPs in the core and $Ru(dpp)_3Cl_2$ in the shell.

3.6 Response time

Using well-established techniques, the N_2 to O_2 and O_2 to N_2 response times were found to be 0.202±0.050 s and 0.404±0.100 s, respectively. This response is largely controlled by the relative O_2/N_2 affinity of the polymers[25] and the amount of time it takes to exchange the gas content in the cuvette containing the fibers.

3.7 Photobleaching

Photobleaching of the three different core-shell configurations was tested in PBS under blue light excitation over a period of one hour of continuous illumination. First, dry scaffolds were attached to the inside wall of cuvette which was then filled with PBS immediately prior to the photobleaching experiment. All three configurations (S1, S2 and S3) demonstrated a minimal loss in signal (<0.8% decrease over one hour), which is within the range of the inherent variations present in the source.

4. Discussion

In creating these core-shell configurations, we hypothesized that a 'handshake' interaction between UCNPs and an oxygen-sensitive complex would be possible. Such a 'handshake' interaction would allow these electrospun core-shell fibers to monitor oxygen concentrations following 980 nm NIR excitation and could potentially extend their oxygen sensing capabilities to biological applications.

Based on our previous work, we chose to utilize a polysulfone (PSU) core and a polycaprolactone (PCL) shell. PSU offers many potential advantages, such as rigidity, toughness, thermal and chemical stability and a high glass transition temperature.[42] Such properties may make it an improved host for the oxygen-sensitive Ru complex. PSU alone can be difficult to electrospin. However, PSU can be easily incorporated into the core of a coaxial fiber, where PCL can be used as the shell for both ease of electrospinning and good biocompatibility.[30,43] Additionally, although we have previously found that $Ru(dpp)_3Cl_2$-containing PCL was not cytotoxic[30], incorporating the Ru complex into a PSU core instead could alleviate the potential for leaching of the oxygen-sensitive molecules over long periods of time.[43] Upconverting nanoparticles have previously been shown to be non-toxic *in vivo* over a period of months by Xiong et al.[44]

Other polymers, such as polydimethylsiloxane (PDMS),[45] offer better oxygen permeability; however, we have demonstrated that the high surface area and short diffusion distances characteristic of electrospun fibers render such materials selection concerns largely irrelevant.[25,30] In addition, the rapid evaporation of solvent during electrospinning allows for homogenous sites for the oxygen-sensing molecules to alleviate concerns surrounding some polymer-probe pairs.[49]

SEM images (Fig. 3) confirm that the ceramic upconverting nanoparticles were successfully incorporated into the electrospun fibers. Backscattered electron images (3B-C) clearly detect aggregates of individual UCNPs having an average diameter of ~135 nm. This is a common observation in many electrospun polymer-ceramic composites[46,47] due to the necessary use of organic solvents that have inherently poor dispersing ability. These should not strongly affect the UCNP output intensity. TEM-CL images (Fig. 4) demonstrate that the incorporated particles are crystalline (via the presence of lattice fringes) and that they are indeed the source of the macroscopically observed luminescence. The cathodoluminescent output consists of the 480 nm UCNP emission as well as a more intense 625 nm $Ru(dpp)_3Cl_2$ output as the $Ru(dpp)_3Cl_2$ molecules within the core were probably also directly excited by the 80 kV illumination.

In this context it was conclusively demonstrated that this ‘handshake’ interaction occurs in this core-shell configuration with varying levels of efficiency. As indicated by the confocal luminescence results (Fig. 5), there are generalized areas of 480 nm emission from UCNPs contained within the fibers upon 980 nm excitation. The widespread blue emission of the UCNPs is sufficient to excite the $Ru(dpp)_3Cl_2$. This ‘handshake’ interaction was demonstrated at a macroscopic level by testing the gaseous oxygen sensing capabilities of the core-shell configurations (Figs. 6 and 7). The oxygen sensing capabilities of these electrospun fibers have been shown to easily extend to dissolved oxygen sensing.[30]

The observed ‘handshake’ interaction begins with 980 nm light absorption by the $LiYF_4$:Yb,Tm UCNPs. Yb^{3+} is the sensitizer ion and absorbs the NIR light in a $^2F_{5/2} \leftarrow {}^2F_{7/2}$ transition. This energy is then transferred to the activator ion Tm^{3+}, which emits blue light centered at 480 nm using the $^1G_4 \rightarrow {}^3H_6$ and $^1D_2 \rightarrow {}^3F_4$ transitions. This blue light is then transferred to the $Ru(dpp)_3Cl_2$ via the ‘handshake’ interaction made possible since both components are in close proximity within electrospun fibers. A metal-to-ligand-charge transfer occurs once the 480 nm light is absorbed by the $Ru(dpp)_3Cl_2$ molecules. This metal-to-ligand-charge transfer ensues when an electron originally contained within

the metal atom's *d* orbital is subsequently transferred into the π^* orbital of the ligand. The subsequent phosphorescent emission is red and is dynamically quenched by the presence of oxygen.

Electrospun core-shell fibers offer many advantages for this design. They allow the UCNPs and oxygen-sensitive complex to be collocated in the same fiber in a variety of configurations. Additionally, a linear Stern-Volmer plot was achieved for gaseous oxygen sensing, which allows for ease of calibration. Although linear Stern-Volmer plots are common for oxygen-sensitive complexes in solution, solid polymer films containing oxygen-sensitive complexes often exhibit a non-linear Stern-Volmer plot. A downward curvature is common as a result of the heterogeneous environment of many polymer films. Therefore, a more complex modified Stern-Volmer relation, such as the two-site model, must be used to describe the oxygen sensing behavior of such films.[2,48] However, the linearity of Fig. 7 indicates that the oxygen sensitive molecules were homogenously incorporated into the electrospun fibers. This parallels earlier observations that the incorporation of oxygen-sensitive molecules into electrospun fibers can achieve a linear Stern-Volmer plot.[25,30,45] Polymer films are the most common hosts for oxygen-sensitive luminescent probes[49] but also suffer from delayed response times. In electrospun scaffolds, small diffusion distances and high surface area allow for a drastically reduced response times as we and others have previously shown.[25,30,45,50,51] The response curve upon switching between oxygen and nitrogen gas has been shown to be rapid and repeatable.[30] Response times for core-shell fibers have been found to be < 0.1 s, short enough to make these sensors useful for real-time, continuous monitoring of oxygen concentration under dynamic conditions.[51]

All three configurations showed appreciable oxygen-sensitive output upon 980 nm excitation. However, the 'handshake' efficiency did vary slightly among these configurations. S1 was the least efficient configuration. It is possible that the collocation of UCNPs and $Ru(dpp)_3Cl_2$ within the core in S1 allowed for $Ru(dpp)_3Cl_2$ agglomeration on the surface of the upconverting particles. $Ru(dpp)_3Cl_2$ can exhibit self-quenching, so agglomeration upon the particle surface could have reduced $Ru(dpp)_3Cl_2$ output. From this consideration, separating the components into the core and shell may provide some advantages. Of these two configurations (S2 and S3), S3 provided the highest 'handshake' efficiency when UCNPs were located in the PSU core and $Ru(dpp)_3Cl_2$ in the PCL shell. One possible explanation for S3's enhanced efficiency versus S2 is that it maximized the amount of oxygen-sensitive red output that could be transmitted from the fiber scaffold without being absorbed by the polymer host. PCL is relatively transparent to 625 nm (~5% absorption), while PSU is less so (~35% absorption).[52,53] Therefore, maximum oxygen-sensitive output involves a configuration that locates UCNPs in the PSU core and $Ru(dpp)_3Cl_2$ in the PCL shell (Figure 8). Further optimization must involve determining the maximum loading of UCNPs achievable in the core and the ideal loading of oxygen sensing complex in the shell. However, there may be some applications in which collocation of both components in the core may be preferred as it could help minimize $Ru(dpp)_3Cl_2$ leaching.[4]

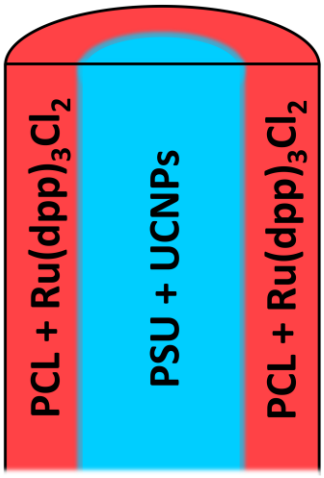

Figure 8: Schematic of most efficient core-shell configuration (S3).

Optical oxygen sensors based on transition metal complexes, such as $Ru(dpp)_3Cl_2$, have many promising qualities, but their reliance on violet or blue excitation wavelengths limits their use in biological applications as such wavelengths undergo high levels of scattering and absorption in biological tissue.[54] Here, we have demonstrated an alternative method to excite $Ru(dpp)_3Cl_2$ using 980 nm NIR light via a 'handshake' interaction with UCNPs in core-shell electrospun fibers. The potential to use such core-shell fibers in biological applications is promising. The red-light output from $Ru(dpp)_3Cl_2$ is absorbed and scattered much less by biological tissue than blue light.[54] While this output exhibits more scattering and auto-fluorescence than the incident 980 nm NIR light, it still falls within the 600-1300 nm "optical window" for optimal detection.[22]

Our main goal in this work was to demonstrate the ability to achieve upconverter-powered oxygen-sensing capabilities within an electrospun fiber format. However, future work will involve attempts to both improve the sensitivity and brightness. New upconverting nanoparticles with greater quantum yields are continually being synthesized[55] and some of these recent strategies could be utilized in this application. These techniques include plasmon-enhanced upconversion[56], dye sensitization antenna strategies[57], the use of different ceramic matrix materials[58], and the implementation of an undoped or "active" (Yb-containing) ceramic shell.[59–61] Although the need for good spectral overlap with the upconverter restricts the possible choices of oxygen-sensitive molecules, we can consider the use of molecules other than $Ru(dpp)_3Cl_2$. For instance, iridium (III) complexes have promising qualities, such as excellent brightness, and some of these complexes have sufficient spectral overlap with the upconverter emission.[62–64] However, Ir(III) compounds generally suffer from poor photostability, an issue that would have to be overcome before they could be used in practical applications.[62,63]

Our future work will also focus on the proposed application of using these sensors for detection of glioma recurrences. We will first assess the feasibility through *in vitro* experiments involving transmission through skull and tissue phantoms. For improved measurement robustness, we plan to explore the idea of ratiometric sensing utilizing the bright 800 nm upconverter emission. We will eventually assess whether the oxygen-sensitive red emission from biosensors located inside living tissue will be able to

adequately exit the tissue for efficient, non-invasive detection in biological applications. If transmission of this red emission becomes an issue a third component – a downconverting particle – would be capable of absorbing the oxygen-sensitive red emission to emit a distinct wavelength of NIR light in return. Another option could be to develop a miniaturized detection array.[65,66]

5. Conclusions

We have demonstrated an alternative method to excite a $Ru(dpp)_3Cl_2$ complex embedded within a polymeric fiber by using 980 nm NIR light to power a 'handshake' interaction with ceramic upconverting nanoparticles (UCNPs) also contained within core-shell electrospun fibers. Additionally, a linear Stern-Volmer plot is achieved for gaseous oxygen sensing allowing for ease of calibration. Such a fiber-based carrier of UCNPs + oxygen-sensitive molecules provides unique opportunities for applications to biological systems. This system may allow investigators to overcome the opacity of living tissues to external illumination sources, because it will generate its own visible light within the target tissue, maximizing the local excitation of the sensing component(s). Moreover, the fiber scaffold will likely recapitulate the topography of the extracellular matrix, facilitating the adhesion and localization of the sensor within the tissue parenchyma and its potential colonization by tumor cells, immune cells, or fibroblasts. SEM and TEM confirmed that the ceramic upconverting nanoparticles were successfully incorporated into the electrospun fibers and remained functional. Gaseous oxygen sensing capabilities were observed, and it was conclusively demonstrated that the envisioned 'handshake' interaction does occur in the designated core-shell configuration at varying levels of efficiency. All three configurations showed appreciable oxygen-sensitive output upon 980 nm excitation. However, the 'handshake' efficiency was highest when the UCNPs were located in the PSU core and $Ru(dpp)_3Cl_2$ in the PCL shell.

For future applications, we propose that UCNP-based nanoscaled sensors (detecting O_2, CO_2, pH and other analytes)[34–36] could provide the basis for a novel type of "smart materials" used to monitor patients using frequent, simple and rapid measures involving minimal clinical intervention.

Acknowledgements

KP acknowledges the generous support of the Department of Defense (DoD) through the National Defense Science & Engineering Graduate Fellowship (NDSEG) Program. This work was supported by research grants from the United States National Science Foundation under Grant Nos. CBET-1033991 and EEC-0425626. We gratefully acknowledge the use of the Leica SP5 Confocal/MultiPhoton microscope within the UCSD School of Medicine Microscopy Core under the auspices of the NINDS P30 core grant (NS047101) Any opinions, findings, and conclusions or recommendations expressed in this material are those of the authors and do not necessarily reflect the views of the National Science Foundation or the National Institutes of Health.

References

[1] S. Heer, K. Kömpe, H.U. Güdel, M. Haase, Highly efficient multicolour upconversion emission in transparent colloids of lanthanide-doped NaYF4 nanocrystals, Adv. Mater. 16 (2004) 2102–2105. doi:10.1002/adma.200400772.
[2] M. Quaranta, S.M. Borisov, I. Klimant, Indicators for optical oxygen sensors, Bioanal. Rev. 4 (2012) 115–157. doi:10.1007/s12566-012-0032-y.
[3] R.M. Clegg, Fluorescence resonance energy transfer, Curr. Opin. Biotechnol. 6 (1995) 103–110. doi:10.1016/0958-1669(95)80016-6.
[4] R. Xue, M.T. Nelson, S.A. Teixeira, M.S. Viapiano, J.J. Lannutti, Cancer cell aggregate hypoxia visualized in vitro via biocompatible fiber sensors, Biomaterials. 76 (2016) 208–217. doi:10.1016/j.biomaterials.2015.10.055.
[5] A.K. Choucair, V. a. Levin, P.H. Gutin, R.L. Davis, P. Silver, M.S.B. Edwards, et al., Development of multiple lesions during radiation therapy and chemotherapy in patients with gliomas, J. Neurosurg. 65 (1986) 654–658. doi:10.3171/jns.1986.65.5.0654.
[6] S.W. Lee, B. a. Fraass, L.H. Marsh, K. Herbort, S.S. Gebarski, M.K. Martel, et al., Patterns of failure following high-dose 3-D conformal radiotherapy for high-grade astrocytomas: A quantitative dosimetric study, Int. J. Radiat. Oncol. Biol. Phys. 43 (1999) 79–88. doi:10.1016/S0360-3016(98)00266-1.
[7] L.E. Gaspar, B.J. Fisher, D.R. Macdonald, D. V. Leber, E.C. Halperin, S.C. Schold, et al., Supratentorial malignant glioma: Patterns of recurrence and implications for external beam local treatment, Int. J. Radiat. Oncol. Biol. Phys. 24 (1992) 55–57. doi:10.1016/0360-3016(92)91021-E.
[8] M.F. Dempsey, B.R. Condon, D.M. Hadley, Measurement of tumor "size" in recurrent malignant glioma: 1D, 2D, or 3D?, AJNR. Am. J. Neuroradiol. 26 (2005) 770–776.
[9] S.M. Evans, B. Joiner, W.T. Jenkins, K.M. Laughlin, E.M. Lord, C.J. Koch, Identification of hypoxia in cells and tissues of epigastric 9L rat glioma using EF5 [2-(2-nitro-1H-imidazol-1-yl)-N-(2,2,3,3,3-pentafluoropropyl) acetamide]., Br. J. Cancer. 72 (1995) 875–882.
[10] D.M. Brizel, S.P. Scully, J.M. Harrelson, M. Brizel, M. Harrelson, J. Layfield, et al., Tumor oxygenation predicts for the likelihood of distant metastases in human soft tissue sarcoma, (1996) 941–943.
[11] L. Yang, C. Lin, L. Wang, H. Guo, X. Wang, Hypoxia and hypoxia-inducible factors in glioblastoma multiforme progression and therapeutic implications, Exp. Cell Res. 318 (2012) 2417–2426. doi:10.1016/j.yexcr.2012.07.017.
[12] K. Lamszus, P. Kunkel, M. Westphal, Invasion as limitation to anti-angiogenic glioma therapye, Acta Neurochir. Suppl. 88 (2003) 169–177.
[13] S.M. Evans, K.D. Judy, I. Dunphy, W. Timothy Jenkins, W.T. Hwang, P.T. Nelson, et al., Hypoxia is important in the biology and aggression of human glial brain tumors, Clin. Cancer Res. 10 (2004) 8177–8184. doi:10.1158/1078-0432.CCR-04-1081.
[14] R.A. Gatenby, H.B. Kessler, J.S. Rosenblum, L.R. Coia, P.J. Moldofsky, W.H. Hartz, et al., Oxygen distribution in squamous cell carcinoma metastases and its relationship to outcome of radiation therapy., Int. J. Radiat. Oncol. Biol. Phys. 14 (1988) 831–838. doi:10.1016/0360-3016(88)90002-8.

[15] A.M. Shannon, D.J. Bouchier-Hayes, C.M. Condron, D. Toomey, Tumour hypoxia, chemotherapeutic resistance and hypoxia-related therapies, Cancer Treat. Rev. 29 (2003) 297–307. doi:10.1016/S0305-7372(03)00003-3.
[16] J.P. Sheehan, M.E. Shaffrey, B. Gupta, J. Larner, J.N. Rich, D.M. Park, Improving the radiosensitivity of radioresistant and hypoxic glioblastoma., Future Oncol. 6 (2010) 1591–1601. doi:10.2217/fon.10.123.
[17] F. Wang, D. Banerjee, Y. Liu, X. Chen, X. Liu, Upconversion nanoparticles in biological labeling, imaging, and therapy., Analyst. 135 (2010) 1839–1854. doi:10.1039/c0an00144a.
[18] H. Guo, H. Qian, N.M. Idris, Y. Zhang, Singlet oxygen-induced apoptosis of cancer cells using upconversion fluorescent nanoparticles as a carrier of photosensitizer, Nanomedicine Nanotechnology, Biol. Med. 6 (2010) 486–495. doi:10.1016/j.nano.2009.11.004.
[19] L. Cheng, C. Wang, Z. Liu, Upconversion nanoparticles and their composite nanostructures for biomedical imaging and cancer therapy, Nanoscale. (2012) 23–37. doi:10.1039/c2nr32311g.
[20] D.K. Chatterjee, M.K. Gnanasammandhan, Y. Zhang, Small upconverting fluorescent nanoparticles for biomedical applications, Small. 6 (2010) 2781–2795. doi:10.1002/smll.201000418.
[21] S. Wu, G. Han, D.J. Milliron, S. Aloni, V. Altoe, D. V Talapin, et al., Non-blinking and photostable upconverted luminescence from single lanthanide-doped nanocrystals., Proc. Natl. Acad. Sci. U. S. A. 106 (2009) 10917–10921. doi:10.1073/pnas.0904792106.
[22] R.R. Anderson, J.A. Parrish, The optics of human skin., J. Invest. Dermatol. 77 (1981) 13–19. doi:10.1111/1523-1747.ep12479191.
[23] L.A. Sordillo, Y. Pu, S. Pratavieira, Y. Budansky, R.R. Alfano, Deep optical imaging of tissue using the second and third near-infrared spectral windows., J. Biomed. Opt. 19 (2014) 056004. doi:10.1117/1.JBO.19.5.056004.
[24] G.M. Hale, M.R. Querry, Optical constants of water in the 200-nm to 200-micron wavelength region., Appl. Opt. 12 (1973) 555–563. doi:10.1364/AO.12.000555.
[25] R. Xue, C. Ge, K. Richardson, A. Palmer, M. Viapiano, J.J. Lannutti, Microscale sensing of oxygen via encapsulated porphyrin nanofibers: effect of indicator and polymer “core” permeability, ACS Appl. Mater. Interfaces. 7 (2015) 8606–8614. doi:10.1021/acsami.5b00403.
[26] S.W. Lai, Y.J. Hou, C.M. Che, H.L. Pang, K.Y. Wong, C.K. Chang, et al., Electronic spectroscopy, photophysical properties, and emission quenching studies of an oxidatively robust perfluorinated platinum porphyrin, Inorg. Chem. 43 (2004) 3724–3732. doi:10.1021/ic049902h.
[27] P.J. Spellane, M. Gouterman, a. Antipas, S. Kim, Y.C. Liu, Porphyrins. 40. Electronic spectra and four-orbital energies of free-base, zinc, copper, and palladium tetrakis(perfluorophenyl)porphyrins, Inorg. Chem. 19 (1980) 386–391. doi:10.1021/ic50204a021.
[28] P.C. Alford, M.J. Cook, A.P. Lewis, G.S.G. McAuliffe, V. Skarda, A.J.. Thomson, et al., Luminescent metal complexes. Part 5. Luminescence properties of ring-substituted 1,10-phenanthroline tris-complexes of ruthenium(II), J. Chem. Soc. Perkin Trans. 2. (1985) 705–709.

[29] W. Cui, Y. Zhou, J. Chang, Electrospun nanofibrous materials for tissue engineering and drug delivery, Sci. Technol. Adv. Mater. 11 (2010) 014108. doi:10.1088/1468-6996/11/1/014108.
[30] R. Xue, P. Behera, M.S. Viapiano, J.J. Lannutti, Rapid response oxygen-sensing nanofibers, Mater. Sci. Eng. C. 33 (2013) 3450–3457. doi:10.1016/j.msec.2013.04.030.
[31] H.J. Yu, S. V. Fridrikh, G.C. Rutledge, Production of submicrometer diameter fibers by two-fluid electrospiiming, Adv. Mater. 16 (2004) 1562–1566. doi:10.1002/adma.200306644.
[32] J. Liu, Y. Liu, W. Bu, J. Bu, Y. Sun, J. Du, et al., Ultrasensitive nanosensors based on upconversion nanoparticles for selective hypoxia imaging in vivo upon near-infrared excitation, J. Am. Chem. Soc. 136 (2014) 9701–9709. doi:10.1021/ja5042989.
[33] R.J. Meier, J.M.B. Simbuürger, T. Soukka, M. Schaüferling, Background-free referenced luminescence sensing and imaging of pH using upconverting phosphors and color camera read-out, Anal. Chem. 86 (2014) 5535–5540. doi:10.1021/ac5009207.
[34] D.E. Achatz, R.J. Meier, L.H. Fischer, O.S. Wolfbeis, Luminescent sensing of oxygen using a quenchable probe and upconverting nanoparticles, Angew. Chemie - Int. Ed. 50 (2011) 260–263. doi:10.1002/anie.201004902.
[35] R. Ali, S.M. Saleh, R.J. Meier, H.A. Azab, I.I. Abdelgawad, O.S. Wolfbeis, Upconverting nanoparticle based optical sensor for carbon dioxide, Sensors Actuators, B Chem. 150 (2010) 126–131. doi:10.1016/j.snb.2010.07.031.
[36] L.-N. Sun, H. Peng, M.I.J. Stich, D. Achatz, O.S. Wolfbeis, pH sensor based on upconverting luminescent lanthanide nanorods., Chem. Commun. (Camb). (2009) 5000–5002. doi:10.1039/b907822c.
[37] W. Lv, T. Yang, Q. Yu, Q. Zhao, K.Y. Zhang, H. Liang, et al., A Phosphorescent Iridium(III) Complex-Modified Nanoprobe for Hypoxia Bioimaging Via Time-Resolved Luminescence Microscopy, Adv. Sci. 201500107 (2015) n/a–n/a. doi:10.1002/advs.201500107.
[38] J. Gaumer, A. Prasad, D. Lee, J. Lannutti, Structure-function relationships and source-to-ground distance in electrospun polycaprolactone, Acta Biomater. 5 (2009) 1552–1561. doi:10.1016/j.actbio.2009.01.021.
[39] J. Nam, Y. Huang, S. Agarwal, J. Lannutti, Materials selection and residual solvent retention in biodegradable electrospun fibers, J. Appl. Polym. Sci. 107 (2008) 1547–1554. doi:10.1002/app.27063.
[40] N. Yamamoto, Development of cathodoluminescence (CL) for semiconductor research, part I: TEM-CL study of microstructures and defects in semiconductor epilayers, in: Y. Watanabe, S. Heun, G. Salviati, N. Yamamoto (Eds.), Nanoscale Spectrosc. Its Appl. to Semicond. Res., Springer-Verlag, Berlin Heidelberg, 2002: pp. 37–51.
[41] D.H. Reneker, A.L. Yarin, Electrospinning jets and polymer nanofibers, Polymer (Guildf). 49 (2008) 2387–2425. doi:10.1016/j.polymer.2008.02.002.
[42] P.M. Hergenrother, The Use, Design, Synthesis, and Properties of High Performance/High Temperature Polymers: An Overview, High Perform. Polym. 15 (2003) 3–45.

[43] R. Xue, Nanofiber Based Optical Sensors for Oxygen Determination, Ohio State University, 2014.
[44] L. Xiong, T. Yang, Y. Yang, C. Xu, F. Li, Long-term in vivo biodistribution imaging and toxicity of polyacrylic acid-coated upconversion nanophosphors, Biomaterials. 31 (2010) 7078–7085. doi:10.1016/j.biomaterials.2010.05.065.
[45] R. Xue, P. Behera, J. Xu, M.S. Viapiano, J.J. Lannutti, Polydimethylsiloxane core-polycaprolactone shell nanofibers as biocompatible, real-time oxygen sensors, Sensors Actuators, B Chem. 192 (2014) 697–707. doi:10.1016/j.snb.2013.10.084.
[46] H. Liu, T.J. Webster, Mechanical properties of dispersed ceramic nanoparticles in polymer composites for orthopedic applications, Int. J. Nanomedicine. 5 (2010) 299–313. doi:10.2147/IJN.S9882.
[47] L.C. Gerhardt, G.M.R. Jell, A.R. Boccaccini, Titanium dioxide (TiO2) nanoparticles filled poly(D,L lactid acid) (PDLLA) matrix composites for bone tissue engineering, J. Mater. Sci. Mater. Med. 18 (2007) 1287–1298. doi:10.1007/s10856-006-0062-5.
[48] E.R. Carraway, J.N. Demas, B.A. Degraff, Luminescence quenching mechanism for microheterogeneous systems, Anal. Chem. 63 (1991) 332–336.
[49] Y. Amao, Probes and polymers for optical sensing of oxygen, Microchim. Acta. 143 (2003) 1–12. doi:10.1007/s00604-003-0037-x.
[50] S.Y. Zhao, B.S. Harrison, Morphology impact on oxygen sensing ability of Ru(dpp)3Cl2 containing biocompatible polymers, Mater. Sci. Eng. C. 53 (2015) 280–285. doi:10.1016/j.msec.2015.04.001.
[51] C. Wolf, M. Tscherner, S. Köstler, Ultra-fast opto-chemical sensors by using electrospun nanofibers as sensing layers, Sensors Actuators B Chem. 209 (2015) 1064–1069. doi:10.1016/j.snb.2014.11.070.
[52] Sigma-Aldrich, Polycaprolactone: FTIR, (n.d.). http://www.sigmaaldrich.com/spectra/ftir/FTIR002053.PDF (accessed September 4, 2015).
[53] Sigma-Aldrich, Polysulfone: FTIR, (n.d.). http://www.sigmaaldrich.com/spectra/ftir/FTIR002083.PDF (accessed September 4, 2015).
[54] A.N. Bashkatov, E.A. Genina, V.I. Kochubey, V. V. Tuchin, Optical properties of human skin, subcutaneous and mucous tissues in the wavelength range from 400 to 2000 nm, J. Phys. D. Appl. Phys. 38 (2005) 2543–2555. doi:10.1088/0022-3727/38/15/004.
[55] X. Li, F. Zhang, D. Zhao, Highly efficient lanthanide upconverting nanomaterials: Progresses and challenges, Nano Today. 8 (2013) 643–676. doi:10.1016/j.nantod.2013.11.003.
[56] Y.-L. Wang, N. Mohammadi Estakhri, A. Johnson, H.-Y. Li, L.-X. Xu, Z. Zhang, et al., Tailoring Plasmonic Enhanced Upconversion in Single NaYF4:Yb(3+)/Er(3+) Nanocrystals., Sci. Rep. 5 (2015) 10196. doi:10.1038/srep10196.
[57] W. Zou, C. Visser, J. a. Maduro, M.S. Pshenichnikov, J.C. Hummelen, Broadband dye-sensitized upconversion of near-infrared light, Nat. Photonics. 6 (2012) 560–564. doi:10.1038/nphoton.2012.158.

[58] Q. Liu, Y. Sun, T. Yang, W. Feng, C. Li, F. Li, Sub-10 nm hexagonal lanthanide-doped NaLuF4 upconversion nanocyrstals for sensitive bioimaging in vivo., J. Am. Chem. Soc. (2011) 17122–17125. doi:10.1021/ja207078s.
[59] F. Vetrone, R. Naccache, V. Mahalingam, C.G. Morgan, J. a. Capobianco, The active-core/active-shell approach: A strategy to enhance the upconversion luminescence in lanthanide-doped nanoparticles, Adv. Funct. Mater. 19 (2009) 2924–2929. doi:10.1002/adfm.200900234.
[60] F. Wang, J. Wang, X. Liu, Direct evidence of a surface quenching effect on size-dependent luminescence of upconversion nanoparticles, Angew. Chemie - Int. Ed. 49 (2010) 7456–7460. doi:10.1002/anie.201003959.
[61] J.-C. Boyer, F.C.J.M. van Veggel, Absolute quantum yield measurements of colloidal NaYF4: Er3+, Yb3+ upconverting nanoparticles., Nanoscale. 2 (2010) 1417–1419. doi:10.1039/c0nr00253d.
[62] S.M. Borisov, I. Klimant, Ultrabright oxygen optodes based on cyclometalated iridium(III) coumarin complexes, Anal. Chem. 79 (2007) 7501–7509. doi:10.1021/ac0710836.
[63] X.D. Wang, H.X. Chen, Y. Zhao, X. Chen, X.R. Wang, X. Chen, Optical oxygen sensors move towards colorimetric determination, TrAC - Trends Anal. Chem. 29 (2010) 319–338. doi:10.1016/j.trac.2010.01.004.
[64] T. Mayr, T. Abel, B. Enko, S. Borisov, C. Konrad, S. Köstler, et al., A planar waveguide optical sensor employing simple light coupling., Analyst. 134 (2009) 1544–7. doi:10.1039/b904536h.
[65] T. Vo-Dinh, ed., Biomedical Photonics Handbook, 1st ed., CRC, Boca Raton, 2003.
[66] J. Tang, L. Wang, J. Ying, W. Lee, P. Ho, Apparatus and methods of using built-in micro-spectroscopy micro-biosensors and specimen collection system for a wireless capsule in a biological body in vivo, US20050154277 A1, 2005.